Journal of Petroleum Exploration and Production Technology
https://doi.org/10.1007/s13202-022-01524-y

ORIGINAL PAPER-EXPLORATION GEOPHYSICS

Pore pressure prediction using seismic acoustic impedance in an overpressure carbonate reservoir

Mohammad Ali Riahi[1] · **Mohammad Ghasem Fakhari**[1]

Received: 16 September 2021 / Accepted: 1 June 2022

Abstract

The drilling engineers favor a quantifiable understanding of the subsurface overpressure zones to avoid drilling hazards. The conventional pore pressure estimation techniques in carbonate reservoirs are prone to uncertainties that affect the calculated pore pressure model resolution and are still far from satisfactory. Basically, in carbonate reservoirs, the effect of chemical process and cementation on porosity is more important than the mechanical compaction, so the conventional pore pressure prediction methods based on the normal compaction trend mostly do not provide acceptable results. Using the conventional methods for carbonate reservoirs can yield large errors, even suggesting a reduction in abnormal pressure in overpressure zones where considerable attention must be paid. Conventional methods need to model density and velocity to calculate the effective and overburden pressures. Converting acoustic impedance to density and velocity is always associated with errors and generally provides low resolution, which adds substantial uncertainties to the pressure prediction. Although pore pressure measurements are usually associated with low resolution, additional error-prone steps can be dropped if used directly. This research outlines the pore pressure estimation of a famous Iranian carbonate reservoir using direct acoustic impedance without inverting it to density and velocity. Finally, this method gives acceptable results in carbonate formations compared to the results of the Repeat Formation Test (RFT) in this region. The results show a zone of overpressure between the two low-pressure intervals of the carbonate reservoir. This result can be of great help in determining reservoir boundaries as well as in planning for drilling trajectory for new wells. Furthermore, the pore pressure estimation results also show pressure reduction in the central part of the seismic section. The proposed approach is a viable alternative to the conventional method and is in line with the geological field report, where the ratio of hydrocarbon potential of total rock on the reservoir sides is higher than its middle part. In this study, we want to emphasize that the calibrated function obtained in our area can be used in similar basins with carbonate reservoirs.

Keywords Acoustic impedance · Carbonate reservoirs · Pore pressure · Post-stack inversion · Repeat formation test (RFT)

Abbreviations

σ_e	Effective stress
σ_{Ov}	Overburden pressure
I_P	Compressional wave acoustic impedance
σ_p	Pore pressure
g	Gravitational constant
Δt_j	Sample interval in the time domain
Δh_j	Sample interval in the depth domain

Introduction

Drilling specialists often need a subsurface pore pressure guide to have safe and efficient drilling. Abnormal pressures (especially overpressure) are serious hazards that can be avoided by knowing the subsurface pore pressure before drilling (Zhang 2011). In addition to drilling hazards, understanding the distribution of overpressure, which origins from disequilibrium compaction of sediments, and determining a high-pressure zone are the important parameters in hydrocarbon exploration. Lots of research has been carried out on the mechanisms of fluid pressure in hydrocarbon reservoirs (Sun et al. 2019, 2021). Concerning fluid flow mechanisms inside shale reservoirs, Sun et al. (2021) investigated a molecular simulation of methane flow behavior through a realistic organic shale matrix under displacement pressure.

✉ Mohammad Ali Riahi
mariahi@ut.ac.ir

Mohammad Ghasem Fakhari
m.gh.fakhari@ut.ac.ir

[1] Institute of Geophysics, University of Tehran, Tehran, Iran

Published online: 24 June 2022

Generally, the most widely used pore-pressure-estimation methods are based on two categories. These methods are based on empirical relationships derived from statistical data or based on laboratory measurements and rock physics models. However, most of these methods employ seismic data for this purpose. One of the earliest methods of pore pressure estimation is the outcome of studies performed by Pennebaker (1968). These studies showed the deviation of the pore pressure indicator from the normal compaction trend line. Effective stress methods: It works through Terzaghi's principle, in which the difference between the total confining stress and the pore pressure controls the sediments' compaction. This method is made up of three steps. (1) Effective stress calculation from pore pressure indicators, (2) bulk density, calculation of the overburden stress. (3) The difference between overburden stress and effective stress gives pore fluid pressure (Das and Mukherjee 2020; Radwan and Sen 2021). Bowers (1995) calculated the effective stress using measured shale pore pressure and overburden pressure (Terzaghi and Peck 1948) and analyzed the corresponding acoustic velocities using the well data in the Gulf of Mexico. Bowers's method is recognized as an effective stress-based approach in which the buried depth and acoustic velocity establish a relationship and are used to estimate the pressure. Consequently, the two mechanisms of loading and non-consolidation are considered. Concerning this relationship, the effective stress outside the velocity inversion zones is calculated from the intact curve. For the zones of velocity inversion case, the well logs should be utilized to determine the correct velocity inversion diagram. Holbrook et al. (2005) presented the porosity-dependent effective stress to predict pore pressures. To estimate the pore pressure using porosity data, Heppard et al. (1998) proposed an empirical relation for porosity similar to Eton′s (1972) method. Zhang (2011) obtained an empirical relation to estimating the pore pressure by using porosity. Raiga-Clemenceau et al. (1988) presented a relation to estimating porosity via p-wave velocity (time-average). They replaced this relation with Zhang's (2011) relation, and they could estimate the pore pressure using either time average or p-wave velocity. Wiley et al. (1956) estimated porosity through an experimentally optimized mean-time relationship. In which, the mean porosity relation of two derived equations is used to calculate the pore pressure and its slope. Unfortunately, pore pressure prediction in carbonate reservoirs using conventional methods is still a challenging task that results in high uncertainties, and so far there is no specific method generally accepted. The effects of chemical process and cementation post diagenesis on porosity are more important than the mechanical compaction in most carbonate rocks, so the conventional pore pressure prediction methods implicitly or explicitly using the normal compaction trend fails to give reliable results (Wang and Wang 2015). Banik et al. (2014) show that the pore pressure can be mainly a function of a single variable (acoustic impedance). They suggested the function $\sigma p = f(Ip)$ is continuous and since the deposition process in different basins or even different regions of a similar basin may be different, they suggest that the parameters defining the function or even the form of the function itself would possibly want to be adjusted in each different zone of interest.

In carbonate reservoirs in field applications, conventional pore pressure prediction methods such as Eaton and Bowers are still used which exposes the well drilling engineering to high risks. The Asmari reservoir is one of the famous Iranian carbonates reservoirs. The main purpose of the current study is to predicate the pore pressure of the Asmari Formation based on acoustic impedance using both seismic data and available well logs located in one of the Iranian oil fields. The workflow of the proposed method is schematically shown in Fig. 1. This figure provides a schematic overview of the prediction of pore pressure directly from the acoustic impedance.

Geological setting

We assess the performance of the pore pressure estimation via acoustic impedance for one of Iran's oil fields. The study oil field is in the dip section of the north of Dezful embayment and about 60 km distance from south Ahwaz. This oil field is constrained to the Ahvaz oil field from northwest and west is close to Ab-Teymor oil field and from the northeast is a juxtaposition with the Shadegan oil field. This oil field was explored by drilling the MI-1 well number in 1963, and

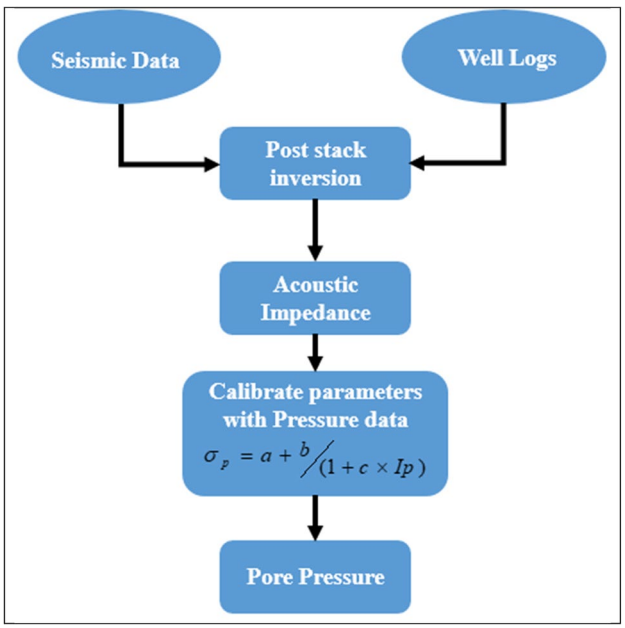

Fig. 1 The workflow illustrates the steps involved in the pore pressure processes algorithm

production from this field was started in 1974. The oil reservoir is under the saturated state, and the primary depth of oil–water contact has been estimated at 2272 m. This oil field comprises Asmari and Bangestan. The Asmari Formation lithology include sandstone, limestone, and dolomite which consists of a double porosity system consisting of fractures and matrices.

Based on the different formations′ surface maps, the Asmari Formation is an asymmetric anticline with a mild 0°–10° slope in the northwest–southeast direction. Depending on the Zagros region′s natural structure, the angle of inclination in the north wing is greater than about 5–6 degrees in the southern flank (Alavi 2004). Although part of the oil and gas are produced from porous layers, most of the production is related to fractures and open cracks. Due to the low slope of the anticlines in Khuzestan, the expansion of the areas with tensile fractures is low, and most of the oil production is from the matrix. This is also true of the Asmari Formation in the studied field. The lithology of the Asmari Formation includes sandstone, shale, and carbonate. Studies of this formation show that this formation has only limited joints and cracks and no fractures. Therefore, it can be concluded that the limited fractures in the carbonate layers do not affect the production of this reservoir (For more information see Alavi 2004).

Methodology

The pore pressure estimation method using acoustic impedance

As mentioned, the estimation of subsurface pore pressure as the pre-drilling analysis is an essential stage in hydrocarbon exploration. Nowadays, methods based on the seismic velocity and a density function are among the most widely used approaches in pore pressure estimation, in which overpressure zone estimation is of interest (Sayers et al. 2002). Of note pore and overpressure, estimation demands the availability of two parameters (velocity and density) in the desired range. Accurate density modeling is one of the most essential tasks in reservoir modeling. However, the accuracy of the density model is often challenged when seismic data alone are inverted for density. Similarly, geostatistical models also face challenges in terms of accuracy, as they frequently require adjustment of the model parameters for each reservoir rock type. The density and velocity are derived from the acoustic impedance of seismic data, in which its conversion to both density and velocity suffers from uncertainties resulting in low resolution estimates. This drawbacks of the conventional approach directly transmit uncertainty into the pressure prediction stage. Furthermore, acoustic impedance resulting from the seismic inversion is much higher with confidence than density (Chatterjee and Yalamanchili 2017).

Rasolofosaon and Tonellot (2011) investigate the impedance-based method for the quantitative evaluation of effective stress and detection of overpressures which shows that the pore pressure can be estimated as a continuous function of acoustic impedance. Consequently, simplifies the process of estimating pore pressure. This method is directly based on acoustic impedance, thereby eliminates the errors due to conversion step.

The Bowers method (Bowers 1995, 2002) showed how pressure could be derived from acoustic impedance as well as estimated density and velocity data based on the cognitive dependence of acoustic velocity on pressure.

$$v = v_0 + a\sigma_e^b \tag{1}$$

$$\sigma_e = \left(\frac{v - v_0}{a}\right)^{\frac{1}{b}} \tag{2}$$

where, σ_e denotes effective stress, and V_0, a, and b are constant parameters.

Bowers (1995) proposed a certain amount of these parameters for his desired marine basin, while these parameters were determined through calibration with pore pressure data at wells in each region.

Multiplying both sides of Eq. 1 with density reads:

$$Ip = Ip_0 + c\sigma_e^b \tag{3}$$

$$\sigma_e = \left(\frac{Ip - Ip_0}{c}\right)^{\frac{1}{b}} \tag{4}$$

which leads to a new equation in terms of acoustic impedance. Banik et al. (2013) described Eqs. 3 and 4 as the modified Bowers' method for effective stress. Likewise, the overburden pressure $\boldsymbol{\sigma_{Ov}}$, generally referred to as the density of sediments on the formation, and can be written as:

$$\sigma_{Ov} = g\sum_j \rho_j \Delta h_j = g\sum_j Ip_j \Delta t_j \tag{5}$$

where, ρ_j and Ip_j are impedance and density; g is the gravitational constant and $\boldsymbol{\Delta t_j}$ and $\boldsymbol{\Delta h_j}$ are the sample intervals in the time and depth domain, respectively. In Eq. 5, the summation performed over all samples collected from the considered formation.

Conventional pore pressure evaluation is primarily based on Terzaghi's (and Biot′s) effective stress principle which states that total vertical stress (σ_{ov}) (or overburden stress) is equal to the sum of the effective vertical stress (σ_e) and the formation pore pressure (σ_p). The Biot's effective stress coefficient (Biot and Willis 1957) alters the

effective stress principle, in which effective stress principle eventually is given by:

$$\sigma_e = \sigma_{Ov} - \alpha\sigma_p \tag{6}$$

where the Biot's stress coefficient of (α) usually is to be 1.because, in sedimentary rocks, this coefficient is assumed to be the same. Banik et al. (2014) show that the pore pressure is mainly a function of a single variable (acoustic impedance). They suggested the function $\sigma p = f(Ip)$ is continuous and since the deposition process may be different in different basins or even different regions (of a similar basin). They suggest that the parameters defining the function or even the form of the function itself would possibly need to be adjusted for each different zone of interest. The function f can be linear or even nonlinear with higher-order polynomials of inverse acoustic impedance in a region with complicated sedimentation processes. In other words, the form of the function and its related parameters need to be adjusted in each region, which is similar to the effective Bower's pressure ratio and velocity ratio, Eq. 1. The parameters V_0, a, and b are varying by region and basin.

Banik et al. (2014) used the subsequent function successfully to convert the inverted acoustic impedance at once into pore-pressure volumes for the deepwater GOM Walker Ridge, Green Canyon, and Keathley Canyon areas:

$$\sigma_p = A + B/I_p \tag{7}$$

where, A and B are transform parameters that need to be determined via the calibration of Eq. 7 in the well located in the same basin with a geologic environment similar to the target area. Banik et al. (2014) calculated effective stress, overburden pressure, and pore pressure directly from the acoustic impedance as well as velocity and density methods (Eaton 1972; Bower 1995) using the above equations for a deep well. They showed that both methods give practically similar results. The pore pressure estimation obtained from the usage of direct impedance can reduce errors due to the conversion of impedance to the density and velocity, and calculate the pore pressure only as a simple single-variable function. In what follows, we utilize the direct impedance method to predict pore pressure in a carbonate reservoir case study.

Available data of the oil filed study

We used 3D migrated seismic data related to the Khami group. The data used in this study are a part of the complete seismic data set of this region, shown in Fig. 2a. As mentioned above, this field′s reservoir ranges from Asmari to the Pabdeh horizon. Seismic horizons can be selected using the information from the wells found in the wells. In Fig. 2b, two important seismic horizons, the Asmari and Pabdeh horizons are shown in the seismic cube.

There are total 60 wells in this field. Due to the range of the reservoir and information related to acoustic, density logs, check shot data, and other information needed, 15 wells were used in this study, in which we used 10 wells due to the completeness of the required information for inversion. As mentioned in the previous sections, to estimate the pressure and calibrate the relationships between pressure and acoustic impedance in this area, the wellbore pressure data are required, RFT data. The remained well logs were used to calibrate the pressure estimation relationship.

Acoustic impedance inversion

One of the important steps in seismic data analysis is to establish the relationship between seismic data and the geological information of the studied area (Avseth et al.

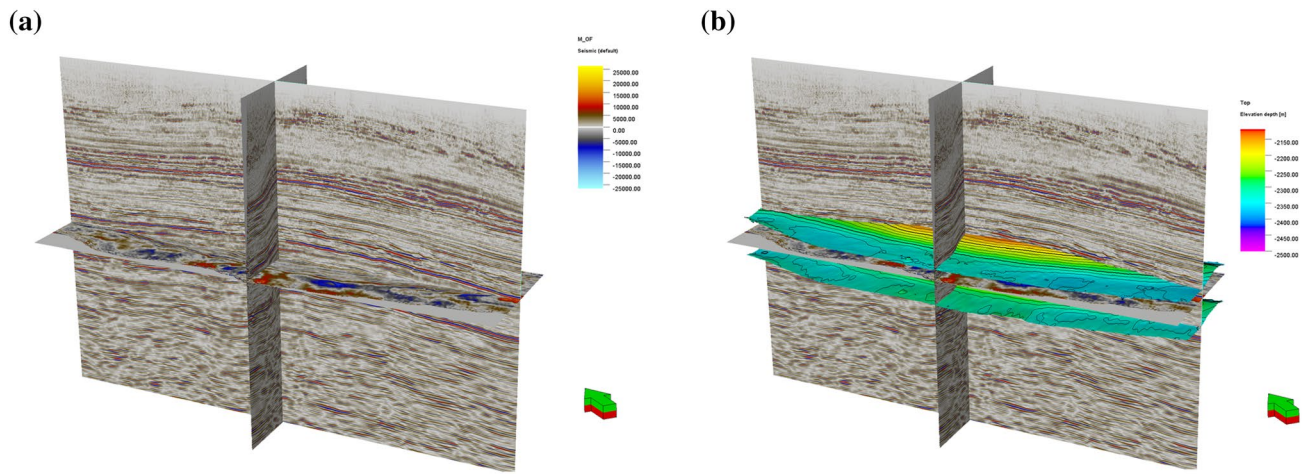

Fig. 2 The seismic cube used in this study. **a** An inline, a crossline, and a z-slice as an instance. **b** The Asmari (upper) and Pabdeh (lower)

2005). Correlation between well logs and seismic data results in identifying and making a correlation between the seismic horizon and the stratigraphy of the reservoir. One of the essential steps before seismological analysis is the depth conversion of the seismic data. The seismic data are recorded in the time domain, however, the well logs are in-depth domain. The common method of interpreting seismic data is to use a synthetic seismogram to match well logs with seismic data. In this study, we used the sonic and density logs of one of the vertical wellbores. Of note that before conducting any evaluation, corrections and depth evaluation of the synthetic seismogram are performed based on check shot and well logs (Rahimi and Riahi 2020). One of the usual methods is to compare seismic traces with the synthetic seismogram at the vertical well locations. In this study, we select the geological horizons (Asmari and Pabdeh Horizon) at the well and then connect the wells to each well by picking the horizon.

Acoustic impedance is the outcome of post-stack inversion. The post-stack seismic inversion technique is the most common approach where high-resolution models of the subsurface are generated, and the effect of the wavelet is eliminated (Chen and Sidney 1997).

There are many post-stack seismic inversion algorithms, in this present study, a Model-based inversion (MBI) algorithm is used. MBI is based on the convolution theory. A simple initial acoustic impedance model is convolved with the wavelet to obtain a synthetic trace compared with the actual seismic trace. (Mallick 1995). Then, this acoustic impedance model is changed iteratively until the resulting synthetic traces are in good agreement with the actual traces. Figure 3 shows the flowchart of the seismic inversion method used in this study.

In this study, the inversion is performed using Hampson Russell software. After estimating an optimal wavelet and building, the initial model inversion is performed by the model-based deterministic method. This method is performed with the Generalized Linear Inversion (GLI) algorithm. The model is modified through iterations until the calculated synthetic traces match with the real seismic traces. The algorithm also adds user-defined constraints such that the updated model lies in a lower–upper bound range. The constraints and user-defined parameters used in this method are reported in Table 1.

Table 1 Parameters and constraints used in our inversion modeling

Average block size	4 ms
Number of iterations	30
Prewhitening	1%
Processing sample rate	4 ms
Constraint	Hard constraint (Lower 100% and Upper 100%)

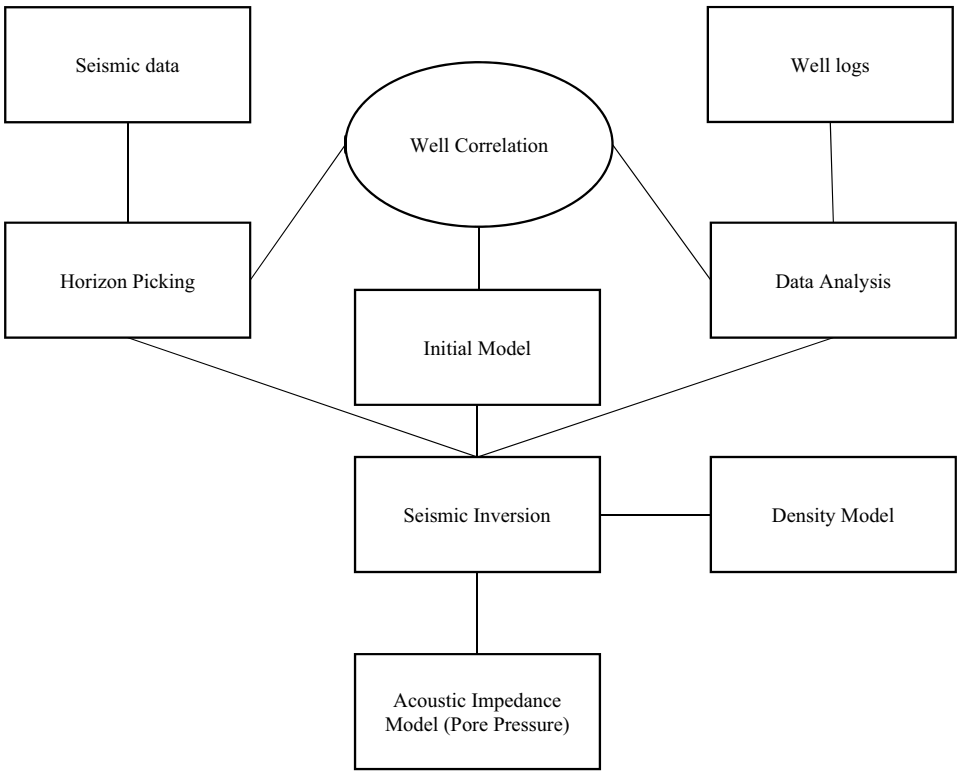

Fig. 3 Flowchart of post-stack seismic inversion used in this study

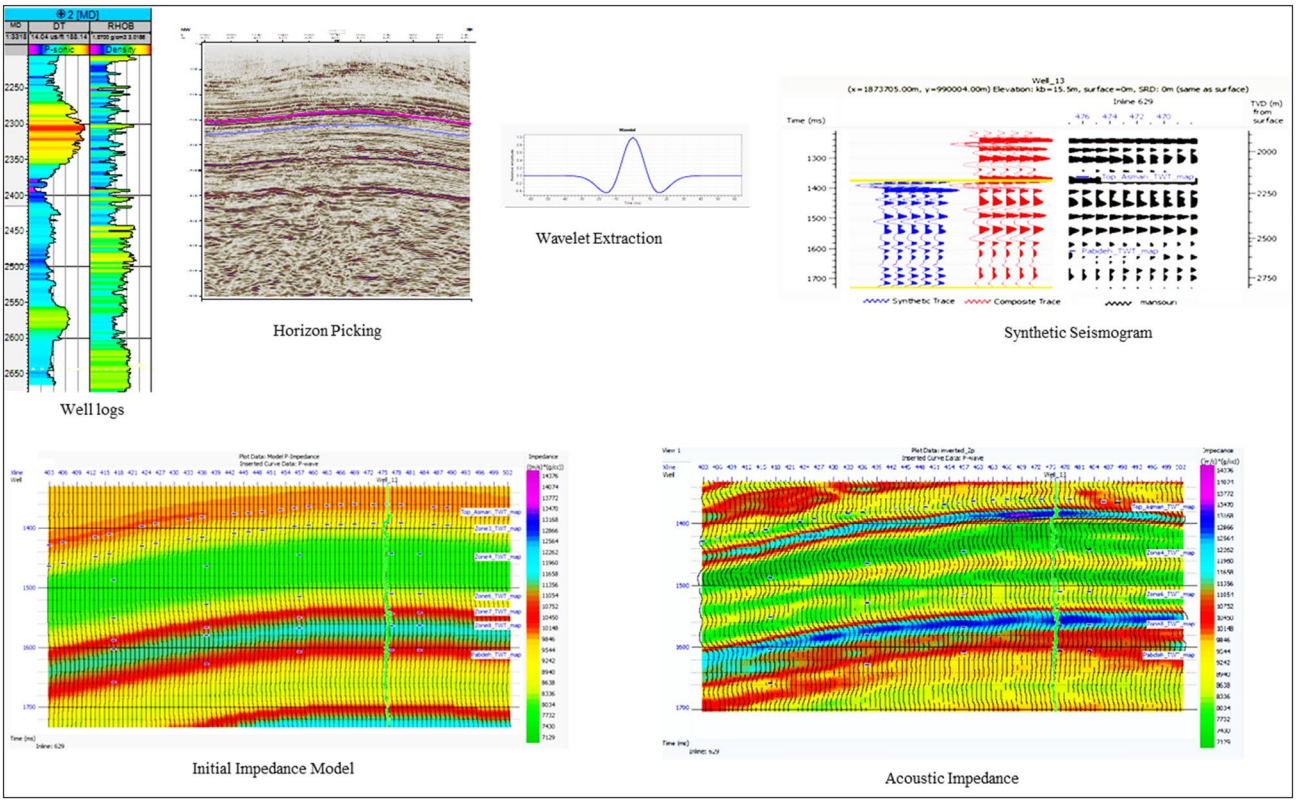

Fig. 4 Schematic of the steps involved in the inversion process

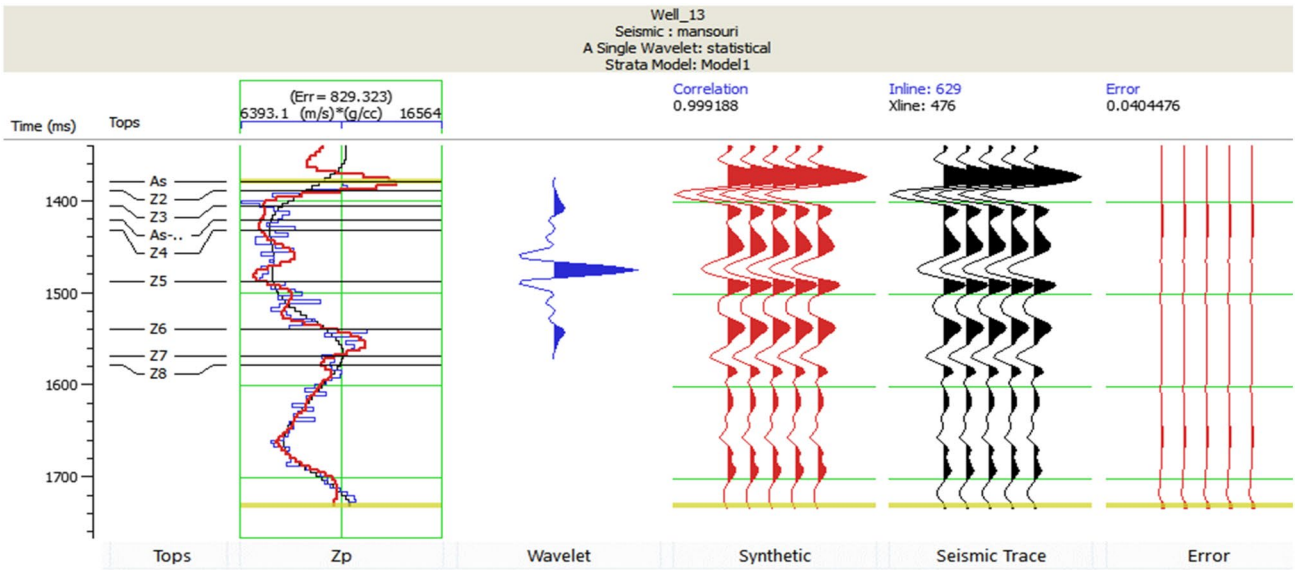

Fig. 5 seismic inversion results in well No. 13. Left curve (red) is overlaid with log-calculated impedance (blue). A Zero-phase wavelet extracted from the seismic cube is shown in the next track. Using impedance from inversion result, reflectivity extracted then convolved with wavelet to generate synthetic trace (red). High correlation with real seismic trace can be interpreted as inversion accuracy. The correlation between the real seismic trace (black) and the synthetic trace (red) is 0.99 at this well location

Figure 4 shows a schematic of the major steps performed in the Inversion process and inversion results for well No. 13 is shown in Fig. 5.

Pore pressure estimation

So far, a cube of acoustic impedance in the reservoir area has been calculated using the seismic inversion process. We continue our analysis to estimate the pore pressure using a direct relation from acoustic impedance, which was discussed in the previous section. To calculate the pore pressure in the study area, we need to find a relationship between calculated acoustic impedance and pore pressure. Here, the following function is used to convert impedance to pore pressure.

$$\sigma_p = a + {}^{b}/_{(1 + c \times Ip)} \tag{8}$$

where, the coefficients a, b, and c are the constant coefficients that must be determined from the calibration of Eq. 8 using pressure data in available wells in this region; Ip and σp are inverted acoustic impedance and pore pressure, respectively.

Having the acoustic impedance determined, pore pressure estimation only requires constant coefficients. The constant coefficients of a, b, and c can be obtained by calibrating this relation at the locations of the wells in which the pressure and impedance values are known. It should be emphasized that to validate and determine the accuracy of the obtained relationship, the predicted pressure from this relation must be compared with the actual pressure. For this purpose, from 5 wells with RFT pressure data available, 3 wells were used to calibrate Eqs. 8, and 2 wells were used for validation and quality control of the method. Therefore, the three wells′ pressure and impedance are used to calibrate Eq. 8. The crossplot of RFT pressure data versus acoustic impedance for each sample of the three wells is shown in Fig. 6.

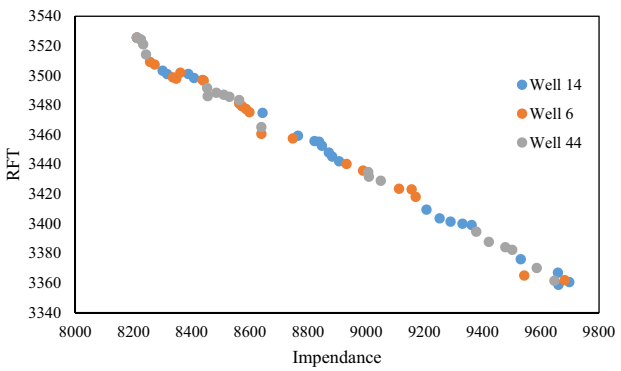

Fig. 6 The crossplot of RFT versus acoustic impedance for three wells

In this step, the MATLAB code and curve-fitting tool are used to calibrate Eq. 8 and determine the constant coefficients. For this purpose, by plotting the RFT via impedance, the desired relation based on relation 8 was obtained, as shown in Fig. 7a. After determining the desired equation, the best line that provides the best fit to the data is obtained based on the minimizing least squares error. Figure 8b shows the coefficients of the best-fitted line.

Figure 8 shows the obtained errors for each sample (distance from the fitted line) and constant coefficients.

After determining the constant coefficients, a simple single-variable equation was obtained wherein the pore pressure is directly dependent only on the inverted acoustic impedance. So, by inserting the inverted impedance value in this calibrated equation can be achieved pore pressure at each point.

Figure 9 shows the acoustic impedance output from the inversion process.

The pressure cube is obtained from the acoustic impedance cube in the same interval, as shown in Fig. 10.

Quality control of impedance pressure relation

Like other modeling processes, quality control of the calculated pore pressure cube seems necessary to validate the results. To this end, wells No. 8 and No.55 that were unused in the procedure is used to assess the pore pressure accuracy.

Accordingly, the pore pressure values obtained using the calibrated pressure-impedance relation is compared with the actual pressure values measured at the wells. Figure 10 shows the results of this comparison which indicates the reliability of the obtained pore pressure model. In this figure, the red dots show the actual measured pressure value at the wells as a function of depth. The blue dots (and continues blue line) show the pore pressure values from the direct pressure-impedance relationship, respectively (Fig. 11).

Here, we performed an uncertainty analysis technique to further evaluate our results. The Standard Error (SE) can be used as a guide to interpreting the possible sampling error. It shows how close the estimate based on sample data might be to the value that would have been taken from the whole population. Confidence intervals use the standard error to derive a range in which expected the true value is likely to lie. A 95% confidence level is frequently used. If a cross plot of samples is drawn and the mean of each calculated, 95% of the means would be expected to fall within the range of two standard errors above and two below the mean of these means. Figure 12 shows the cross plot of acoustic impedance and pore pressure values with error bars and 95% confidence intervals.

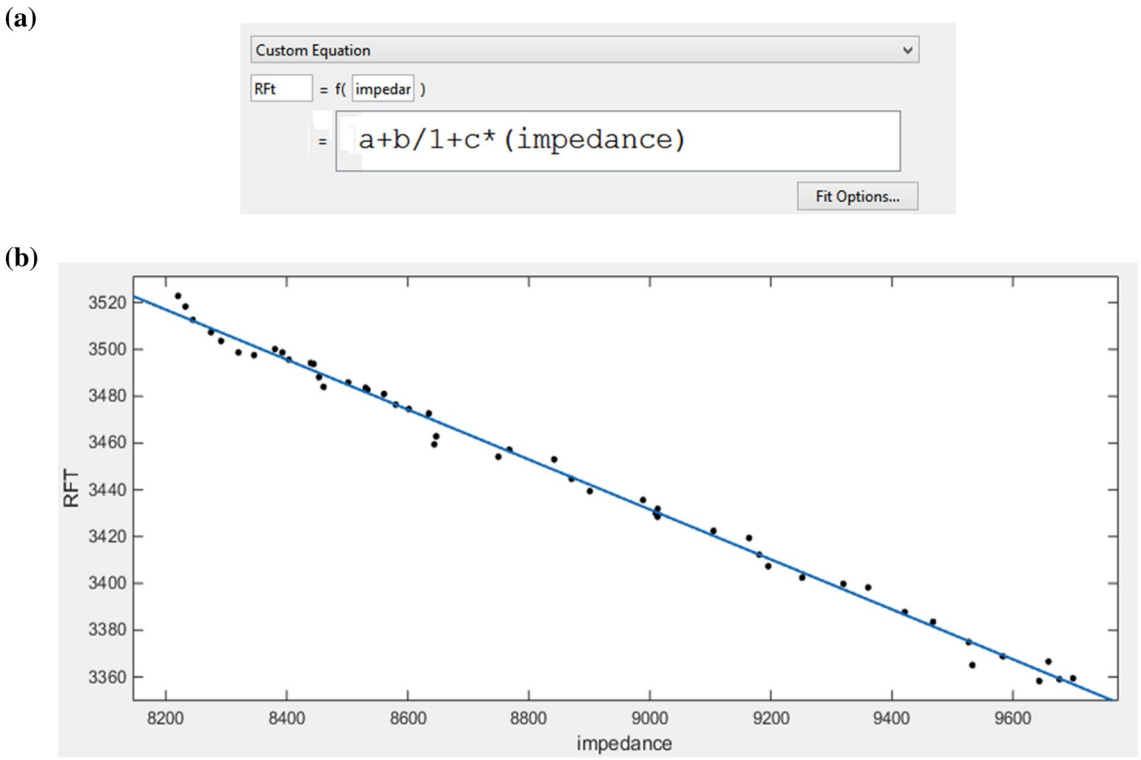

Fig. 7 curve-fitting tool. **a** Insert the desired equation as an arbitrary equation to fit the curve onto the data. **b** The best fit line to the data is based on the equation shown above

Discussion of the results of the estimated pore pressure

In the process of predicting a parameter, it may seem sufficient to test the results alone with the test data. Here, by excluding pressure data for wells No. 8 and No. 55 from all stages of the project and comparing the results obtained for these two wells with the true pore pressure values, the estimation was validated. Since the direct estimation of pressure on acoustic impedance is considered in this study, validation of inversion and impedance determination results is also important. In the section on the determination of acoustic impedance from inversion, a quantitative analysis of inversion results was performed. Here, too, it is appropriate to review the results qualitatively. The 2D cross section of inverted impedance is shown in Fig. 13. In terms of interpretability and qualitative results, it is expected that at the top and bottom of the reservoir (Asmari and Pabdeh horizon) there are two layers of high acoustic impedance, as shown in Fig. 13, with the highest acoustic impedance in this interval. There are two horizons, and within the reservoir interval, as expected, the acoustic impedance value is low, thus showing the interpretability of the acoustic impedance results and the inversion accuracy.

Figure 14a shows the pore pressure corresponding to the desired cross section (Crossline 403). It is to be expected that pore pressure increase in the reservoir. In other words, it is expected that there exists an overpressure interval between two low-pressure confined layers as shown in Fig. 14. Figure 14b shows a Z slice in the reservoir interval. It can be seen that pressure decrease in the central part of this section, which is also consistent with the geological report of the field, where the ratio of hydrocarbon potential to total rock on both sides of the reservoir is better than the middle part of it. Another validation of the results is the pressure estimation.

In Fig. 15, a 3D image of the cube obtained for pore pressure is shown: Inline, Crossline, and Z Slice in time scale.

Therefore, in terms of interpretability and qualifications, the results are accepted by qualitative and interpretative analysis. Figure 14 shows that a zone of overpressure between the two low-pressure layers of the reservoir. This result can be of great help in determining reservoir boundaries as well as in planning for drilling trajectory for

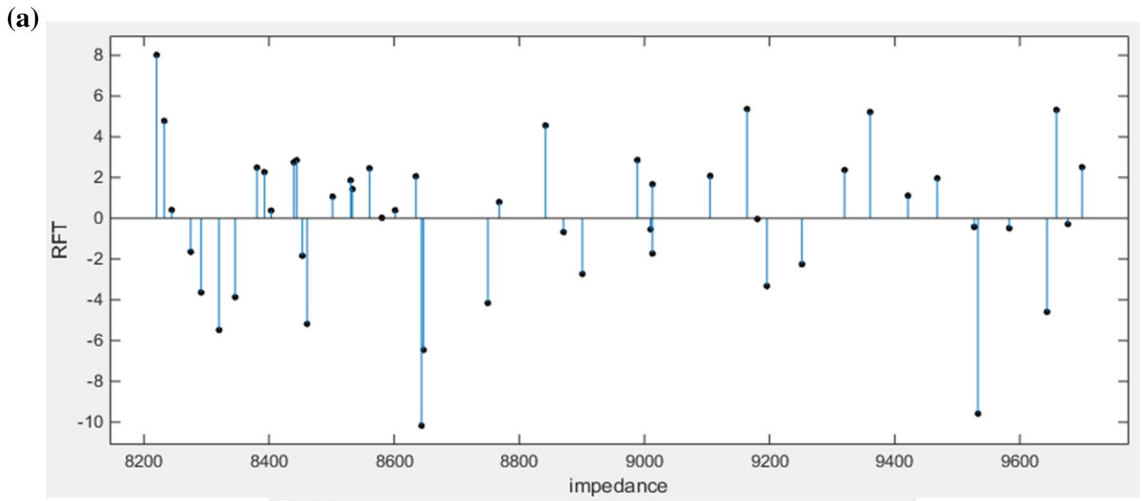

Fig. 8 **a** The error bars of each sample data from the fitted line showing each data′s error. **b** Fixed coefficients **a**, **b** and c after calibration and curve-fitting on data

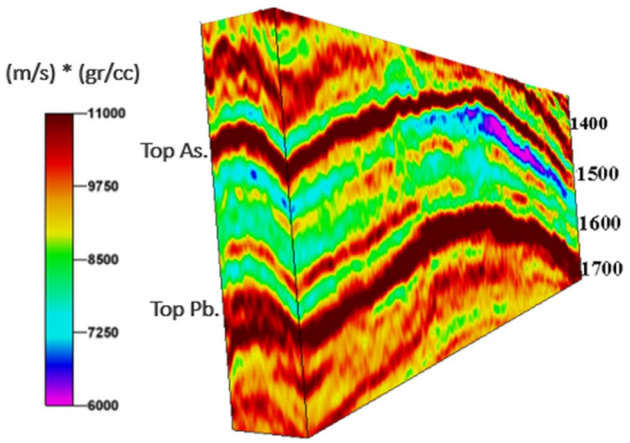

Fig. 9 Acoustic impedance cube

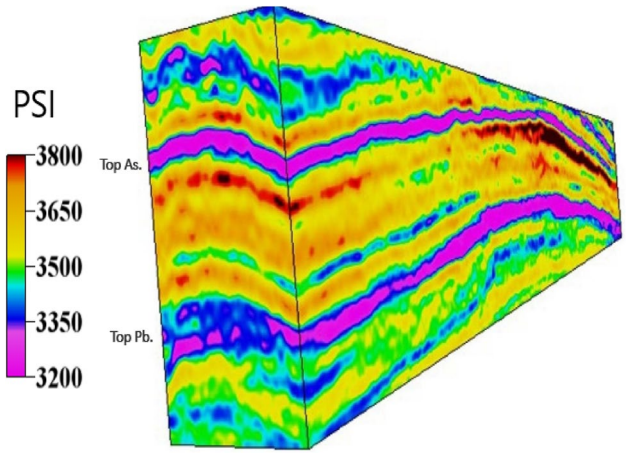

Fig. 10 Pressure cube calculated from acoustic impedance with the calibrated parameters

new wells. As a complementary study, the results show a decrease in pressure in this section′s central part relative to the surrounding area. This feature is consistent with the oil field′s geological report, where the hydrocarbon potential of total rock on both sides of the reservoir is higher than the middle part of the reservoir. Besides, the pore pressure estimation results in this study can determine the weight of the

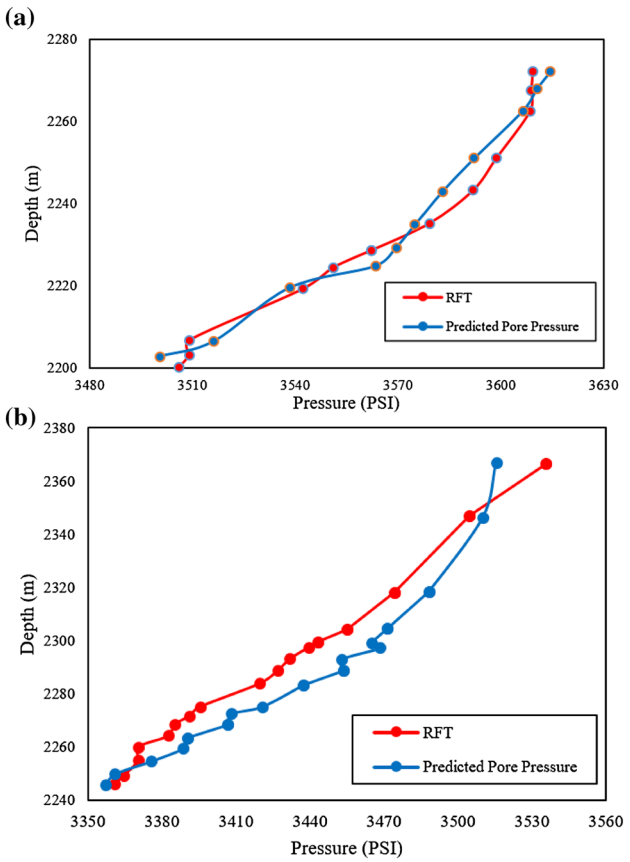

Fig. 11 Comparison of estimated pore pressure values (blue line) and RFT values at a) well 8 and **b** well 55

drilling mud window required in the drilling design of new wells. Concerning the pore pressure cube obtained in this study, it can be concluded that less drilling mud reservoir is needed in the central part of the Z slice section. Other results that may be plausible in this study are observations of high-pressure regions where their pressure is close to the reservoir pressure, which may indicate reservoir leakage and fluid migration in these areas. The formation pressure assessment regulates the weight of the drilling mud and studies the reservoir, and fluid migration is required.

Concluding remarks

Pore pressure estimation is an important issue in improving oil field exploration and drilling projects. The commonly used pressure estimation methods are methods that calculate pore pressure from estimated velocity equations, such as Eaton's method, which requires both the density and velocity information obtained by acoustic impedance inversion, and suffer from conversion errors. In this study, we directly estimated pore pressure based on an impedance-based method to directly predict pore pressure using the seismically derived acoustic impedance and prevent the additional errors and uncertainty due to converting acoustic impedance into density and velocity cubes. We assessed this method for one of Iran's oil fields. We obtained an acoustic impedance cube from seismic data

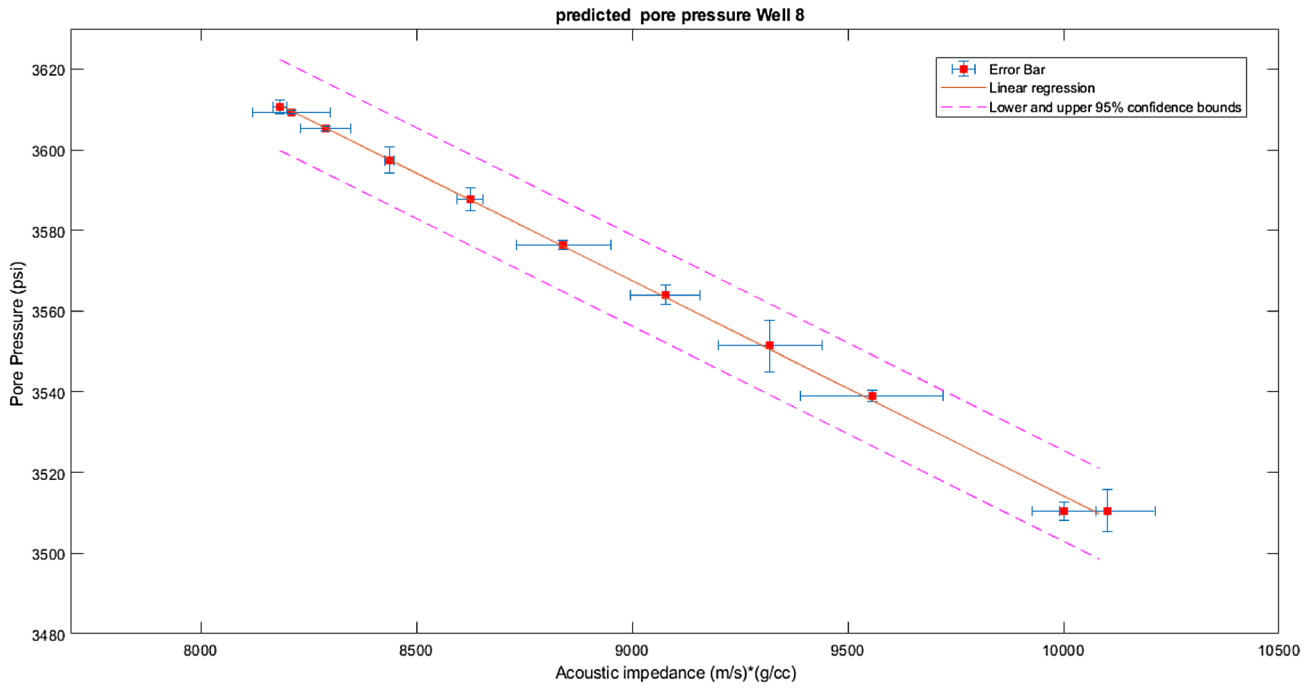

Fig. 12 The uncertainty analysis of predicted pore pressure using direct acoustic impedance. The X and Y axes are acoustic impedance and pressure values, respectively. Also, the solid and dashed lines are linear regression and 95% confidence intervals, respectively

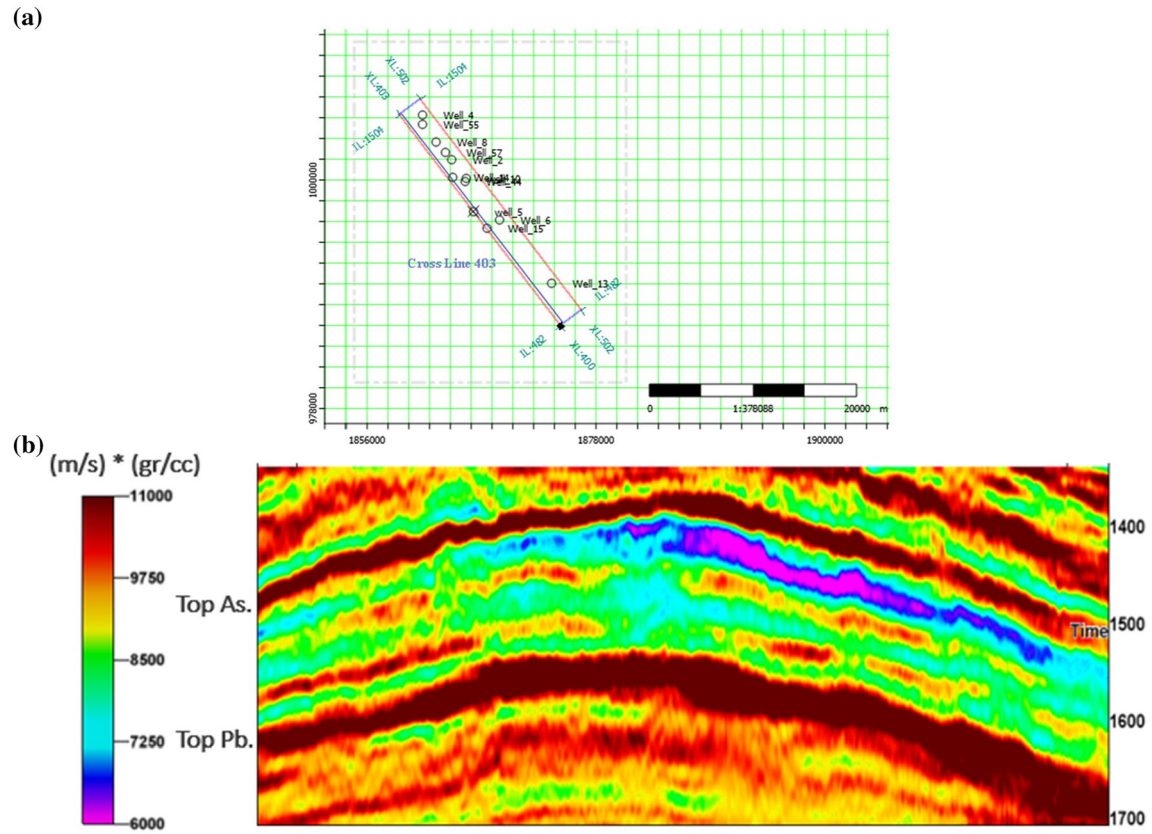

Fig. 13 **a** Base map of the study area showing well locations. Note: the seismic crossline that was discussed is in thick blue (Crossline 403). **b** Inversion of acoustic impedance in cross-section 403

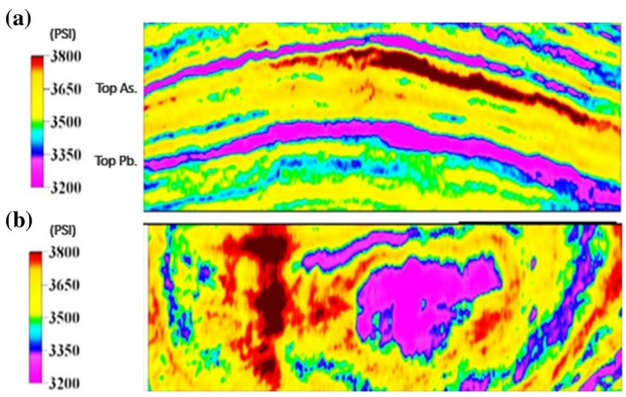

Fig. 14 **a** Pore pressure obtained from the acoustic impedance of the crossline 403. **b** Pore pressure obtained from acoustic impedance at Z slice in time scale

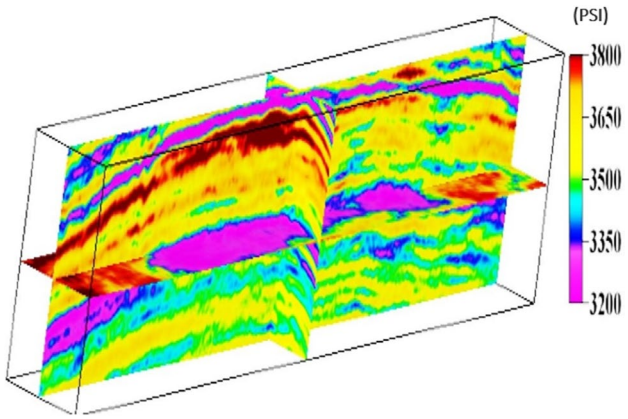

Fig. 15 3D volume obtained for pore pressure in three directions inline, crossline, and Z slice in time scale

inversion, using a simple transformation function to convert the acoustic impedance to pore pressure, and calibrate this relationship with multi-well pressure data. The results are evaluated qualitatively and quantitatively. The measured pressure from RFT in the two wells No. 8 and No. 55, in which their data were not involved in any computation steps, has acceptable accuracy compared to our predicted pore pressure in these wells. In terms of interpretability and qualifications, results are also accepted by qualitative and interpretative analysis. The results show a zone of overpressure between the two low-pressure layers of the

reservoir. This result can be of great help in determining reservoir boundaries as well as in planning for drilling trajectory for new wells. The results of this study reflect that acoustic impedance data through the integrated post-stack inversion scheme are needed for impedance-based pore-pressure prediction.

Acknowledgements The authors acknowledge the research council of the University of Tehran. We acknowledge the journal, two anonymous reviewers, for their insightful comments.

Funding This research did not receive any specific grant from funding agencies in the public, commercial, or not-for-profit sectors.

Declarations

Conflict of interest On behalf of all authors, the corresponding author states that there is no conflict of interest.

References

Abdel-Fattah M, Tawfik A (2015) 3D geometric modeling of the abu madi reservoirs and its implication on the gas development in Baltim area. Offshore Nile Delta, Egypt

Alavi M (2004) Regional stratigraphy of the Zagros fold-thrust belt of Iran and its proforeland evolution. Am J Sci 304(1):1–20

Atashbari V, Tingay MR (2012) Pore pressure prediction in a carbonate reservoir. In: SPE oil and gas India conference and exhibition. Society of petroleum engineers, Mumbai, India. doi: https://doi.org/10.2118/150836-MS

Avseth P, Mukerji T, Mavko G (2005) Quantitative seismic interpretation—applying rock physics tools to reduce interpretation risk. Cambridge University Press, Cambridge

Banik N, Koesoemadinata A, Wagner C, Inyang C, Agarwal V, Priezzhev I (2014) Predrill prediction of subsalt pore pressure from seismic impedance. Leading Edge 33(4):400–412

Banik N, Koesoemadinata A, Wagner C, Inyang C, Bui H (2013) Predrill pore-pressure prediction directly from seismically derived acoustic impedance, Conference: SEG, At: Houston, TX, USA

Biot MA (1941) General theory of three-dimensional consolidation. J Appl Phys 12(2):155–164

Biot M, Willis D (1957) The elastic coefficient of the theory of consolidation. J Appl Mech 24:594–601

Bowers GL (1995) Porepressure estimation from velocity data: accounting for overpressure mechanism beside undercompactions: SPE drilling and complication, June, 89–95

Bowers GL (2002) Detecting high overpressure: the leading edge, February, 174–177

Chatterjee, S., & Yalamanchili, S. R. (2017, September). Density from wave impedance by seismic inversion: a new approach for gravity aided modeling. In: 2017 SEG International exposition and annual meeting. OnePetro

Chen Q, Sidney S (1997) Seismic attribute technology for reservoir forecasting and monitoring. Lead Edge 16:445–456

Das T, Mukherjee S (2020) Pore Pressure Determination Methods, Chapter January 2020. https://www.researchgate.net/publication/332381362, doi: https://doi.org/10.1007/978-3-030-13442-6_3

Dasgupta T, Mukherjee S (2020) Detection of abnormal pressures from well logs. Sediment compaction and applications in petroleum geoscience. Springer, Cham, pp 31–49

Dutta NC (1987) Geopressure. Soc Pet Eng, Geophys, Reprint Ser. No7

Eaton, BA (1972) Graphical method predicts geopressure worldwide: World Oil, June, 51–56

Fertl WH (1976) Abnormal formation pressure. Elsevier, Amsterdam, p 385

Fertl WH, Chapman RE, Holz RF (1994) Studies in abnormal pressure. Elsevier, Amsterdam

Heppard PD, Cander HS, Eggertson EB (1998) Abnormal pressure and the occurrence of 760 hydrocarbons in offshore eastern Trinidad, West Indies, in Law, B.E., G.F. Ulmishek, and V.I. Slavin 761 eds., Abnormal pressures in hydrocarbon environments: AAPG Memoir 70, p 215–246

Holbrook PW, Maggiori DA, Hensley R (2005) Real-time pore pressure and fracture gradient 763 evaluation in all sedimentary lithologies. SPE Form Eval 10(4):215–222

John A, Soni M, Gaur M, Kothari V (2017) AAPG GTW oil and gas resources of India: exploration and production opportunities and challenges. Mumbai, India, pp 6–7

John A, Kumar A, Karthikeyan G, Gupta P (2014) An integrated pore pressure model and its application to hydrocarbon exploration: a case study from the Mahanadi Basin, east coast of India. In: Paper appears in interpretation, vol 2, Society of Exploration Geophysicists and American Association of Petroleum Geologists, pp SB17–SB26

Lahann RW, Swarbrick RE (2011) Overpressure generation by load transfer following shale framework weakening due to smectitediagenesis. Geofluids 11:362–375

Mallick S (1995) Model-based inversion of amplitude-variations-with-offset data using a genetic algorithm. Geophysics 60:939954

Pennebaker ESJr (1968) Seismic data depth magnitude of abnormal pressure: World Oil, June, 73–77

Radwan A, Sen S (2021) Stress path analysis for characterization of in situ stress state and effect of reservoir depletion on present-day stress magnitudes: reservoir geomechanical modeling in the gulf of Suez Rift basin. Egypt Nat Resour Res 30:463–478

Rahimi M (2020) Riahi MA (2020) Static reservoir modeling using geostatistics method: a case study of the Sarvak formation in an offshore oilfield. Carbon Evap 35:62. https://doi.org/10.1007/s13146-020-00598-1

Raiga-Clemenceau J, Martin JP, Nicoletis S (1988) The concept of acoustic formation factor for 794 more accurate porosity determination from sonic transit time data. Log Anal 29(1):54–60

Rasolofosaon P, Tonellot T (2011) Method for quantitative evaluation of fluid pressures and detection of overpressures in an underground medium, US Patent 7,974,785

Sayers CM, Johnson GM, Denyer G (2002) Predrill pore pressure prediction using seismic data. Geophys 67:1286–1292

Sun Z, Shi J, Wu K, Zhang T, Feng D, Xiangfang L (2019) Effect of pressure-propagation behavior on production performance: implication for advancing low-permeability coalbed-methane recovery. SPE J. 24:681–697

Sun Z, Huang B, Li Y, Lin H, Shi S, Yu W (2021) Nanoconfined methane flow behavior through realistic organic shale matrix under

displacement pressure: a molecular simulation investigation. J Pet Explor Prod Technol 12(4):1193–1201

Terzaghi K, Peck RB (1948) Soil mechanics in engineering practice. Wiley, New York, NY, p 566

Tingay M, Morley C, Laird A, Limpornpipat O, Krisadasima K, Suwit P, Macintyre H (2013) Evidence for overpressure generation by kerogen-to-gas maturation in the northern Malay basin. AAPG Bull 97:639–672

Wang Z, Wang R (2015) Pore-pressure prediction using geophysical methods in carbonate reservoirs: status, challenges, and way ahead. J Nat Gas Sci Eng 27:986993

Wylie MRJ, Gregory AR, Gardner LW (1956) Elastic wave velocities in heterogeneous and porous media. Geophys 21:41–70

Zhang J (2011) Pore pressure prediction from well logs: methods, modifications, and new approaches. Earth-Sci Rev 108:50–63